

Microphysical analysis of supercell rear-flank downdrafts using dual-polarization radar observations

Matthew R. Kumjian and Alexander V. Ryzhkov

CIMMS, University of Oklahoma, and NOAA/OAR/National Severe Storms Laboratory, Norman, OK

1. Introduction

Recent research has shown that tornadic and nontornadic supercell storms are virtually indistinguishable in their radar appearances (e.g., Trapp 1999, Wakimoto and Cai 2001). In a large observational project (VORTEX1; Rasmussen et al. 1994) only subtle differences were found. For example, Trapp (1999) found that the mesocyclones in tornadic supercells had slightly greater vertical vorticity and smaller core radii than nontornadic mesocyclones. More attention has been given to the observational results of Markowski et al. (2002), Shabbott and Markowski (2006), Grzych et al. (2007), and the modeling study of Markowski et al. (2003), which show that tornadogenesis appears to be sensitive to thermodynamic characteristics of the rear-flank downdraft (RFD; for a review of RFDs, see Markowski [2002]). Specifically, supercells that produced significant tornadoes had RFDs with smaller equivalent potential temperature θ_e and virtual potential temperature θ_v deficits than nontornadic supercell RFDs.

The RFD thermodynamic properties are driven mainly by microphysical processes such as evaporation of hydrometeors. For the first time, this study analyzes the RFDs of three tornadic and three nontornadic supercells using dual-polarization radar observations, which are sensitive to phase transitions such as melting and evaporation. We attempt to find any systematic differences in the polarimetric properties in the RFD between tornadic and nontornadic storms.

In the next section the data and methodology used in this analysis are discussed. Section 3 presents an overview of the changes in polarimetric variables at low levels leading up to tornadogenesis. The fourth section describes the quantitative analysis of tornadic and nontornadic RFDs, highlighting differences found in the polarimetric data and providing physical interpretations for these differences. A brief discussion and the conclusions drawn from this study are presented in Section 5.

2. Data and Methods

Data were collected by the polarimetric prototype WSR-88D in Norman, Oklahoma. For the tornadic cases (8 May 2003, 10 May 2003, and 30 May 2004) the volume scan immediately preceding tornadogenesis was selected. For the nontornadic cases (20 May 2003, 26 May 2004, and 11 April 2007), the chosen volume scan coincided with a time when the storm looked capable of producing a tornado. In other words, the time was selected if a cyclonically curved “hook” echo appendage was present with low-level rotation. In some cases, the volume scan was selected if the local National Weather Service forecast office issued a tornado warning for the storm. The lowest available elevation angle

that was not contaminated with ground clutter was used. In all cases, the elevation angle was chosen such that the storm was being sampled at a height of about 1 km or less. This was done to obtain data representative of near-surface conditions in the storm.

Low-level PPIs were constructed for each of the storms at the times leading up to tornadogenesis to evaluate the evolution of polarimetric characteristics in and around the RFD. For the quantitative analysis of the RFDs, the data bins within the RFD were isolated. This was done by subjectively identifying the RFD and hook echo from the PPI plots and selecting only data bins that were within this region; care was taken not to include the FFD. Also, the times of tornadic cases were chosen so that no tornadic debris would be present in the hook echo. Tornadic debris has very distinct and dominant polarimetric characteristics and is not representative of the hydrometeors in the hook echo (Ryzhkov et al. 2005a). In addition to the analysis of each individual case, hook echo data from the three tornadic cases are concatenated, as are the three nontornadic cases. This is done to reduce the effects of the variability from storm to storm.

The polarimetric variables utilized in the analysis are radar reflectivity factor at horizontal polarization Z_{HH} , differential reflectivity Z_{DR} , co-polar cross-correlation coefficient at zero lag time ρ_{HV} , and specific differential phase K_{DP} . However, instead of directly comparing the K_{DP} to other variables such as Z_{HH} , the rainfall rates computed from K_{DP} and Z_{HH} are employed. Following Ryzhkov et al. (2005b),

$$R(Z_{HH}) = 1.7 \cdot 10^{-2} \cdot 10^{0.0714 Z_{HH}} \quad (1)$$

where Z_{HH} is in dBZ and R is in mm hr^{-1} , and

$$R(K_{DP}) = 44.0 |K_{DP}|^{0.822} \text{sgn}(K_{DP}) \quad (2)$$

where K_{DP} is in deg km^{-1} . This is a more meaningful comparison than the raw Z_{HH} and K_{DP} values. Note that hail contamination is possible, so we do not claim that these are accurate *rainfall rates*, rather it is simply a convenient way to compare the variables.

The results of the analysis are presented in the following sections.

3. Evolution of Polarimetric Features

In general, the Z_{HH} core in the FFD shifts towards the rear of the storm with time leading to tornadogenesis. This is likely associated with the occlusion of the updraft and the rearward shift of the vertical vorticity maximum to encompass the updraft and downdraft in the “divided mesocyclone” phase (Lemon and Doswell 1979). The Z_{DR} arc (Kumjian and Ryzhkov 2008a,b) increases in magnitude and coverage, extending closer to the updraft and becoming more curved in appearance. The edge of the low-level FFD echo also tends to become more concave. In the RFD and

hook echo, the magnitude of Z_{DR} decreases slightly and K_{DP} increases in extent. In at least two cases (8 May and 10 May) ρ_{HV} slightly increases. Overall, the hook echo becomes more cyclonically curved in times leading to tornadogenesis. These findings are consistent with the preliminary climatology offered in Van Den Broeke et al. (2008). Physically, these changes in the characteristics of the RFD are consistent with a surging cascade of precipitation wrapping around the low-level mesocyclone. It also possibly indicates that the amount of evaporation is limited, since a decrease in Z_{DR} and an increase in ρ_{HV} mean a decrease in the relative contribution from larger drops in the backscattered signal. The addition of smaller drops broadens the DSD, increasing K_{DP} . For excessive evaporation, smaller drops would be lost, increasing Z_{DR} and decreasing K_{DP} . The response of the polarimetric radar variables to such evaporation should be quantified in an attempt to distinguish tornadic RFDs from nontornadic RFDs in the context of the recent VORTEX1 findings.

4. Quantitative Analysis

First, the height of the radar beam is calculated to ensure the storm is sampled in the lowest 1 km above the ground. The calculation was performed following Doviak and Zrnić (1993),

$$h \approx \sqrt{r^2 + (k_e a)^2} + 2rk_e a \sin(\phi_e) - k_e a + h_{\text{radar}} \quad (3)$$

where r is the radial range of the sampling volume, ϕ_e is the elevation angle of the radar beam, a is the earth's radius, h_{radar} is the height of the radar antenna above the ground, and k_e is the effective earth radius coefficient. Here we assume $k_e = 4/3$, which is reasonable for low altitudes, low elevation angles, and where the vertical gradient of refractivity is constant. For the supercell cases, the data is from late afternoon in a well-mixed boundary layer, so a small constant refractivity gradient is a tolerable assumption. The calculated beam heights are shown in Table 1 below. All of the data are from at or below about 1 km.

| Date | T/N | Time (UTC) | El. | Approximate Beamheight |
|---------------|-----|------------|-------|------------------------|
| 8 May 2003 | T | 2157 | 1.5° | 693 m |
| 10 May 2003 | T | 0157 | 0.5° | 1011 m |
| 20 May 2003 | N | 0021 | 0.0° | 740 m |
| 26 May 2004 | N | 2352 | 0.44° | 552 m |
| 30 May 2004 | T | 0155 | 0.0° | 200 m |
| 11 April 2007 | N | 0009 | 0.0° | 383 m |

Table 1: List of storm cases and information about the volume scans for the data utilized in the analysis. The elevation angle of the radar (El.) is given along with the approximate height of the beam that sampled the hook echo.

Because of the wide scatter of the data, “median lines” are constructed. For every 2-dBZ interval of Z_{HH} (from 30 – 32 dBZ to 54 – 56 dBZ), the median value of the polarimetric variable of interest is calculated. These median values are then connected to form the median lines of $Z_{HH} - Z_{DR}$ and $Z_{HH} - \rho_{HV}$ for each storm.

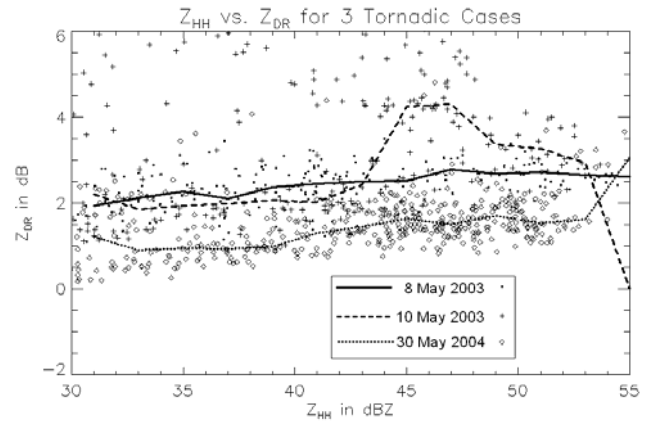


Fig. 1: Data points for the 3 tornadoic cases along with the median lines: 8 May 2003 (dots and solid line), 10 May 2003 (plus signs and dashed line), and 30 May 2004 (diamonds and dotted line), for the $Z_{HH} - Z_{DR}$ data.

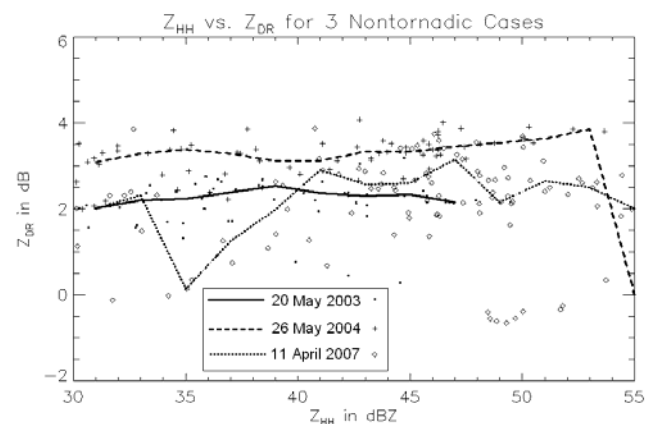


Fig. 2: As in Fig. 1, except for the 3 nontornadoic cases: 20 May 2003, 26 May 2004, and 11 April 2007.

As expected, there exists a substantial amount of variability from storm to storm. Figure 1 shows the $Z_{HH} - Z_{DR}$ data from the three tornadoic storms (the three nontornadoic storms are presented in a similar manner in Fig. 2). Median lines of Z_{DR} are separated by as much as 1 dB. The comparative lack of data points for some cases causes the median lines to fluctuate more widely than other cases. Similarly, Figures 3 and 4 show the $Z_{HH} - \rho_{HV}$ scatterplots and median lines for each of the three tornadoic and nontornadoic storms, respectively. The tornadoic cases (Fig. 3) exhibit much less variability than for the $Z_{HH} - Z_{DR}$ case (Fig. 1). The median lines for 8 May 2003 and 30 May 2004 are remarkably similar for Z_{HH} greater than about 37 dBZ. In all cases, ρ_{HV} remains fairly high (~ 0.98), even for higher Z_{HH} . This indicates a fairly broad spectrum of raindrops and probably little or no hail. The nontornadoic cases (Fig. 4) exhibit greater variability, part of which is likely due to the comparatively fewer data points than the tornadoic cases. The median lines appear to be lower than the tornadoic cases, which could indicate a greater contribution from large drops in the sampling volume (i.e., a more narrow spectrum or one skewed towards larger drops) and/or the presence of some hail.

Next, the concatenated (“tornadoic” and “nontornadoic” datasets, herein T and NT, respectively) are compared. The

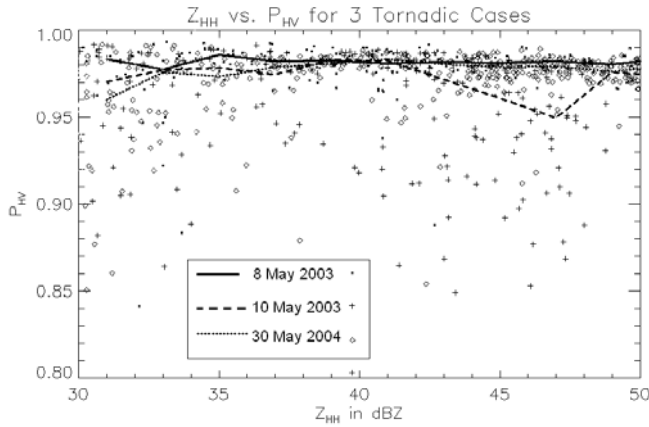


Fig. 3: As in Fig. 1, except for the $Z_{HH} - \rho_{HV}$ data.

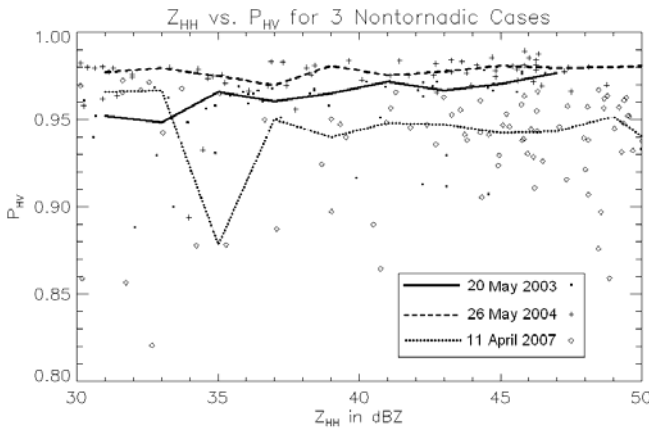


Fig. 4: As in Fig. 2, except for the $Z_{HH} - \rho_{HV}$ data.

concatenation of multiple storm cases for both categories allows for less variable median lines, whereby producing better method of comparing the two categories. In the $Z_{HH} - Z_{DR}$ scatterplot, we find considerable overlap (Fig. 5). Nonetheless, there is a systematic difference between the median Z_{DR} value for each 2-dBZ Z_{HH} interval for T and NT storms. This difference is physically consistent with recent observational research. The NT data show higher Z_{DR} for a given Z_{HH} than the T data. This indicates a larger median drop size, possibly indicating greater evaporation rates. There is a remarkable difference in the slope of the $Z_{HH} - Z_{DR}$ scatter for both NT and T storms compared to normal rainfall events in Oklahoma. Figure 6 overlays the Z_{DR} median lines from NT and T storms and the $Z_{HH} - Z_{DR}$ relation for Oklahoma precipitation (Cao et al. 2008):

$$Z_{DR} = 10^{(-2.6857 \cdot 10^{-4} Z_{HH}^2 + 0.04892 Z_{HH} - 1.4287)} \quad (4)$$

The RFD curves are much flatter than the normal rain scatter, indicating that both NT and T RFDs generally contain more large drops than ordinary rain cases, especially for lower Z_{HH} regimes. Violent airflow in supercells causes more size sorting, especially in the strong gradient of vertical velocity found between the updraft and downdraft. This size sorting leads to a larger median drop size, especially in low- Z_{HH} regions and along gradients of Z_{HH} (Kumjian and Ryzhkov 2008b).

Comparing the $Z_{HH} - \rho_{HV}$ scatter, we also find a difference in the NT and T data (Fig. 7). Tornadoic RFDs are characterized by higher ρ_{HV} than nontornadoic RFDs. Again, this finding is physically consistent with the notion that greater evaporation in nontornadoic RFDs leads to a narrowing of the DSD. At S band, backscatter differential

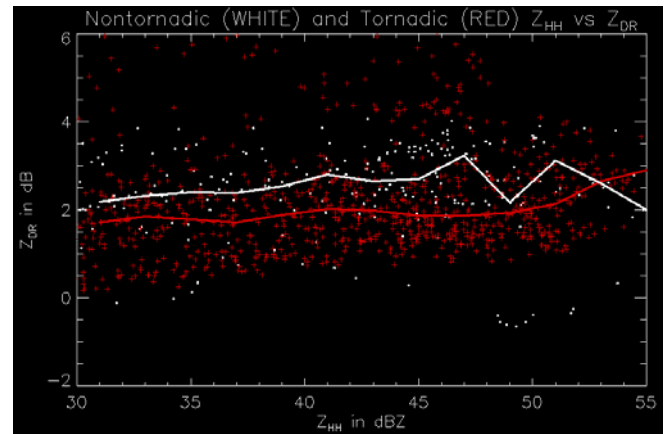


Fig. 5: $Z_{HH} - Z_{DR}$ scatterplots for the concatenated tornadoic and nontornadoic datasets. Tornadoic data are indicated by red crosses (+) and nontornadoic data are white dots. The thick solid lines are curves showing the median Z_{DR} value for each 2-dBZ Z_{HH} interval.

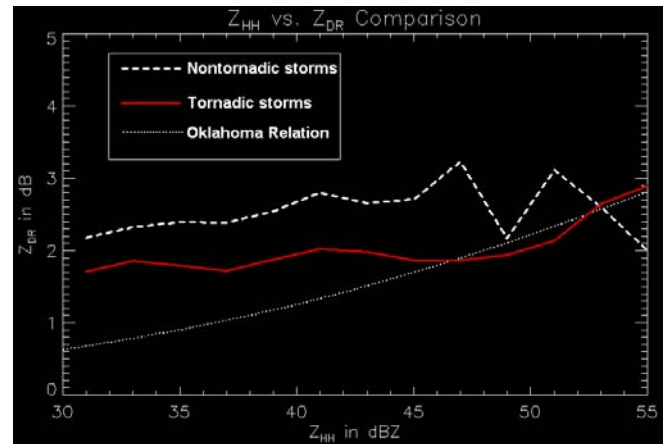


Fig. 6: Median $Z_{HH} - Z_{DR}$ lines for nontornadoic storm RFDs (white dashed line), tornadoic storm RFDs (red solid line), and the Oklahoma relation from Cao et al. (2008; white dotted line).

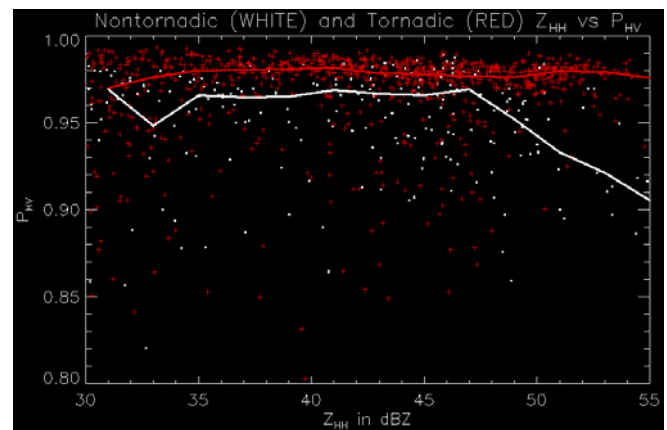


Fig. 7: As in Fig. 5, but for $Z_{HH} - \rho_{HV}$.

phase becomes nonzero for large (6 – 8 mm) drops. Thus, for greater contributions from large drops in the resolution volume (implying a relative lack of smaller drops), the ρ_{HV} should be slightly lower. At C band, where backscatter differential phase is significant for large drop sizes, this effect should be more prominent. Hail in the RFD could also contribute to the lower ρ_{HV} in NT storms, but it is

unclear why NT storms would be more conducive to having hailstones in this part of the storm.

The comparison between NT and T $R(Z_{HH})$ and $R(K_{DP})$ is more difficult to interpret (Fig. 8). Again we see evidence of a DSD skewed to larger sizes in the RFD since a majority of the data points lie below the one-to-one line. The addition of more data may highlight any trends that are not discernable at the present.

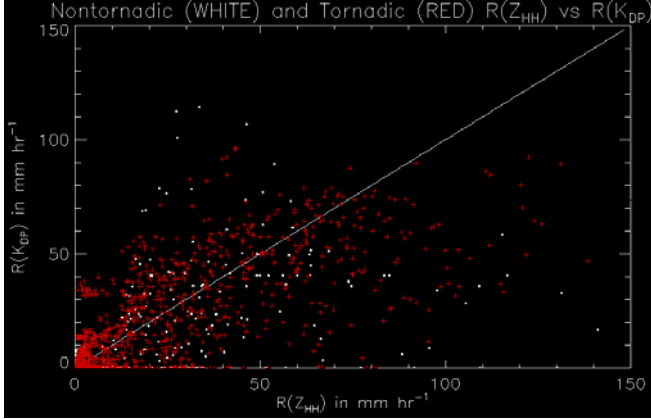


Fig. 8: Scatterplot of the $R(Z_{HH})$ - $R(K_{DP})$ relation for tornadic (red) and nontornadic (white) storms. The one-to-one line indicating where $R(Z_{HH})$ and $R(K_{DP})$ are the same is shown for comparison.

5. Conclusions

Differences in the thermodynamic characteristics of RFDs of T and NT storms found in recent studies are driven by microphysical properties of the RFD. The microphysical differences are governed by the rate of evaporation, which in principle should be manifest in polarimetric radar observations. Such differences in the polarimetric characteristics between T and NT storms are found. To quantify these differences, we define the difference between the NT and T median lines, Δ , for both Z_{DR} and ρ_{HV} . The median and mean of Δ are summarized in Table 2.

| | $\Delta(Z_{DR})$ | $\Delta(\rho_{HV})$ |
|---------------|------------------|---------------------|
| Median | 0.66 dB | 0.016 |
| Mean | 0.52 dB | 0.024 |

Table 2: Statistics quantifying the difference between the nontornadic and tornadic median lines for the $Z_{HH} - Z_{DR}$ scatterplot and the $Z_{HH} - \rho_{HV}$ scatterplot. The values given are the median difference and mean difference between the median lines using the magnitude of NT - T data.

However, these findings are *not* statistically significant, owing to the large scatter of measurements and the small sample size. Though further cases may improve the statistical significance of these results, we do not expect that these differences will be discernable in the operational setting. On the other hand, the addition of more cases may further obscure the differences. Nonetheless, the results are physically consistent with other recent observations and may aid in improving microphysical parameterizations. Simple real-time modeling of the lowest 1 km of the atmosphere initialized with the precipitation distribution inferred from polarimetric measurements may improve short-term forecasts of tornadoes in supercells. Trends in polarimetric characteristics of the RFD may alert forecasters

to impending tornadogenesis, improving nowcasts and increasing the warning lead time.

6. Acknowledgements

This work is part of a Ph.D. dissertation at the University of Oklahoma and is partially supported under the NSF grant ATM-0532107. Additional funding comes from NOAA/Office of Oceanic and Atmospheric Research under NOAA-University of Oklahoma Cooperative agreement #NA17RJ1227, U.S. Department of Commerce.

7. References

- Cao, Q., G. Zhang, E. Brandes, T. Schuur, A.V. Ryzhkov, and K. Ikeda, 2008: Analysis of video disdrometer and polarimetric radar data to characterize rain microphysics in Oklahoma. *J. Appl. Meteor. and Climatology*, **in press**.
- Doviak, R.J. and D.S. Zrnić, 1993: *Doppler Radar and Weather Observations*. Academic Press, 562 pp.
- Grzych, M.L., B.D. Lee, and C.A. Finley, 2007: Thermodynamic analysis of supercell rear-flank downdrafts from project ANSWERS. *Mon. Wea. Rev.*, **135**, 240-246.
- Kumjian, M.R. and A.V. Ryzhkov, 2008a: Polarimetric signatures in supercell thunderstorms. *J. Appl. Meteor. and Climatology*, **in press**.
- Kumjian, M.R. and A.V. Ryzhkov, 2008b: Microphysical size sorting revealed from dual-polarization Doppler radar. Extended Abstracts, *88th Annual AMS Meeting, New Orleans*, Amer. Meteor. Soc., P2.13.
- Lemon, L.R. and C.A. Doswell, 1979: Severe thunderstorm evolution and mesocyclone structure as related to tornadogenesis. *Mon. Wea. Rev.*, **107**, 1184-1197.
- Markowski, P.M., 2002: Hook echoes and rear-flank downdrafts: A review. *Mon. Wea. Rev.*, **130**, 852-876.
- Markowski, P.M., J.M. Straka, and E.N. Rasmussen, 2002: Direct surface thermodynamic measurements within the rear-flank downdrafts of nontornadic and tornadic supercells. *Mon. Wea. Rev.*, **130**, 1692-1721.
- Markowski, P.M., J.M. Straka, and E.N. Rasmussen, 2003: Tornadogenesis resulting from the transport of circulation by a downdraft: Idealized numerical simulations. *J. Atmos. Sci.*, **60**, 795-823.
- Rasmussen, E.N., J.M. Straka, R.P. Davies-Jones, C.A. Doswell III, F.H. Carr, M.D. Eilts, and D.R. MacGorman, 1994: The Verifications of the Origins of Rotation in Tornadoes Experiment: VORTEX. *Bull. Amer. Meteor. Soc.*, **75**, 997-1006.
- Ryzhkov, A.V., T.J. Schuur, D.W. Burgess, and D.S. Zrnić, 2005a: Polarimetric tornado detection. *J. Appl. Meteor.*, **44**, 557-570.

- Ryzhkov, A.V., T.J. Schuur, D.W. Burgess, P.L. Heinselman, S.E. Giangrande, and D.S. Zrnich, 2005b: The Joint Polarization Experiment. *Bull. Amer. Meteor. Soc.*, **86**, 809-824.
- Shabbott, C.J. and P.M. Markowski, 2006: Surface in situ observations within the outflow of forward-flank downdrafts of supercell thunderstorms. *Mon. Wea. Rev.*, **134**, 1422-1441.
- Trapp, R.J., 1999: Observations of nontornadic low-level mesocyclones and attendant tornadogenesis failure during VORTEX. *Mon. Wea. Rev.*, **127**, 1693-1705.
- Van Den Broeke, M.S., J.M. Straka, and E.N. Rasmussen, 2008: Polarimetric radar observations at low-levels during tornado life cycles in a small sample of classic Southern Plains supercells. *J. Appl. Meteor.*, **in press**.
- Wakimoto, R.M. and H. Cai, 2001: Analysis of a nontornadic storm during VORTEX 95. *Mon. Wea. Rev.*, **128**, 565-592.